Ising lines: Natural topological defects within ferroelectric Bloch walls

V. Stepkova, P. Marton, and J. Hlinka*
Institute of Physics, Czech Academy of Sciences, Na Slovance 2, 18221 Praha 8, Czech Republic
(Received 6 March 2015; revised manuscript received 1 May 2015; published 16 September 2015)

Phase-field simulations demonstrate that the polarization order-parameter field in the Ginzburg-Landau-Devonshire model of rhombohedral ferroelectric $BaTiO_3$ allows for an interesting linear defect, stable under simple periodic boundary conditions. This linear defect, here called the Ising line, can be described as an about 2-nm-thick intrinsic paraelectric nanorod acting as a highly mobile borderline between finite portions of Bloch-like domain walls of opposite helicity. These Ising lines play the role of domain boundaries associated with the Ising-to-Bloch domain-wall phase transition.

DOI: 10.1103/PhysRevB.92.094106 PACS number(s): 77.80.Dj, 77.84.−s

I. INTRODUCTION

Perovskite ferroelectrics are the key materials in current ferroelectric research, and a considerable effort was recently devoted to investigations of their domain structure and their domain-wall properties. Much less is known about ferroelectric line defects, although this topic is now gaining attention [1–11], for example, in relation to magnetic vortices and skyrmions [1,2]. Ferroelectric domains and line defects are inspiring in other research areas, too, for example, in the particle physics [12].

Here we demonstrate that perovskite ferroelectrics like $BaTiO_3$ may contain an interesting linear defect, analogous to the edge dislocation lines of crystal lattices and twist disclination lines of liquid-crystal textures [13,14] but related to the vectorial field of the spontaneous polarization. It is similar to magnetic Bloch and Néel lines [15–18], but the ferroelectric line obtained here has a vanishing polarization at the axis of its core (see Fig. 1). Therefore, we will denote the specific defect studied here as an *Ising line*.

This Ising line is ultimately related to the existence of *ferroelectric Bloch walls*, recently inferred from phenomenological [19–22] and first-principles calculations [23,24] for $BaTiO_3$ and $PbTiO_3$. In particular, within the Ginzburg-Landau-Devonshire (GLD) model of Refs. [25,26], the Bloch-like (bistable and chiral) structure of the $[\bar{2}11]$-oriented 180° domain wall of rhombohedral $BaTiO_3$ has been demonstrated [19,22]. Moreover, this wall can be transformed to an achiral, Ising-like domain wall, for example, by moderate uniaxial stress [21]. The transformation proceeds as a continuous, symmetry-breaking phase transition associated with a divergence of the dielectric permittivity [27] and with a disappearance of the polarization $\mathbf{P}_{DW}$ *within the domain-wall interior* [21]. The "internal" polarization $\mathbf{P}_{DW}$ of the Bloch wall between domains with spontaneous polarization parallel and antiparallel to the [111] direction is parallel or antiparallel to the $[0\bar{1}1]$ direction (we refer to the cubic axes of the parent phase; see Fig. 2).

In light of these findings, we expect that the simple array of 180° Ising walls depicted in Fig. 2(a) is unstable at ambient pressure. In phase-field simulations, a minor perturbation typically transforms the structure of Fig. 2(a) into an array of Bloch walls, for example, the one in Fig. 2(b), where the $\mathbf{P}_{DW}$ vector has opposite orientation within neighboring domain walls [21]. Such a domain structure contains only the domain walls of the same helicity, and it is thus a chiral structure as a whole, but there are no defect lines there. Obviously, it can be anticipated that the antiparallel $\mathbf{P}_{DW}$ states could coexist within the same domain-wall plane, similar to how the ferroelectric domains may coexist in the bulk ferroelectric crystal [22,28–30]. Then, soliton-like line defects with a characteristic profile may form at the borderline between domain-wall regions of opposite helicity, similar to how the Bloch or Néel lines may form within magnetic Bloch walls [22,30].

Here we report a domain structure with equal left-handed and right-handed areas within each Bloch-wall plane, which is numerically stable in the standard phase-field GLD simulations for $BaTiO_3$. This racemic structure, depicted in the Figs. 2(d)–2(f), indeed comprises a set of Ising lines, such as that in Fig. 1. The aim of this paper is to describe their basic properties.

II. PHASE-FIELD SIMULATIONS

The present phase-field simulations employed a phenomenological GLD energy functional complemented by exact calculation of the long-range electrostatic energy associated with the inhomogeneous profile of the polarization field [31]. The local mechanical equilibrium and strain compatibility are implicitly imposed by the method [31]. Further details about the phase-field approach in ferroelectrics can be found in Refs. [6,26,32–34]. In the results displayed here, we used the same GLD model parameters for $BaTiO_3$ as in Ref. [21]. The adjustable temperature parameter of the model was set to 118 K, but similar results were obtained at other temperatures within the stability range of the rhombohedral ferroelectric phase. Periodic boundary conditions were applied to both polarization and strain fields. Furthermore, the overall stress-free conditions were assumed (stress averaged over the periodic supercell is vanishing). The calculation was typically conducted on a $128 \times 128 \times 128$ discrete mesh with 0.5- or 0.25-nm spatial steps. This allows us to inspect local polarization vectors at the scale of the perovskite elementary unit-cell parameter (see Fig. 3).

The initial configuration had a steplike polarization seed profile in which polarization directions roughly conform to that

*hlinka@fzu.cz

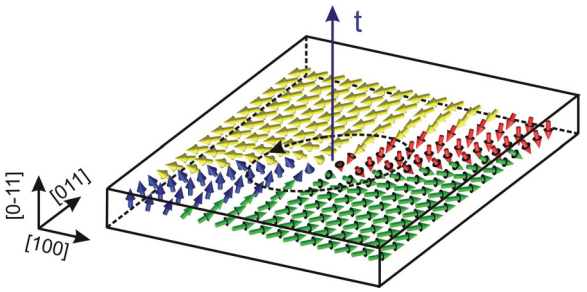

FIG. 1. (Color online) Ising line defect in rhombohedral $BaTiO_3$ as obtained from the model described in the text. When circumventing the core of this defect following a closed path (dashed line) around its axis **t**, the polarization on this path rotates around the $[\bar{2}11]$ axis, which is *perpendicular* to **t**.

in Figs. 2(d)–2(f). A careful design of the initial configuration was an essential condition for keeping the Ising lines in the relaxed domain structure because these lines are highly mobile and easily annihilate. The architecture of our initial configuration obviously respected the basic requirements such as that the energetically very costly head-to-head or tail-to-tail polarization configurations should be avoided. Among other things, this implies that the Ising lines are all parallel to $\mathbf{P}_{DW}$ [see Figs. 2(c) and 2(e)].

Subsequently, the initial polarization field configuration has been fully relaxed according to the time-dependent Ginzburg-Landau equation [21,26,31]. The final relaxed domain-structure state indeed kept the overall architecture of the engineered initial state [Fig. 2(d)], at least as long as the distances between the Ising lines were larger than about 3 nm and the distance between the domain walls was larger than about 6 nm. Such polarization profiles can be viewed as the exact numerical solution of the Euler-Lagrange equations of the above-introduced GLD model.

III. RESULTS

The local arrangement of the polarization in the relaxed structure around the core of the Ising line is shown in Fig. 3. The structure can be best understood in terms of the symmetry-adapted coordinates associated with the orthogonal unit vectors $\mathbf{r} \parallel [111]$, $\mathbf{s} \parallel [\bar{2}11]$, and $\mathbf{t} \parallel [0\bar{1}1]$ shown in Fig. 2(c). For example, the Bloch nature [21,35] of the domain walls becomes apparent when the P_r, P_t, P_s polarization components are traced across the domain wall [see Fig. 4(a)]: In the heart of the domain wall, the principal polarization component P_r passes through zero, but the additional polarization component P_t appears, so that the total polarization at the $P_r = 0$ point is nonzero. The exchange between P_r and P_t components on the path across the domain wall corresponds to the rotation of the polarization vector within the plane parallel to the domain wall. In the domain walls shown in Fig. 4(b), the polarization rotates in the same sense as the windings on a right-handed screw; the opposite sense of rotation is encountered in domain walls depicted in Fig. 4(a).

Figure 4(c) displays the polarization profile along a trajectory that connects the antiparallel bulk domain states through the Ising line. It demonstrates that within the Ising line, the

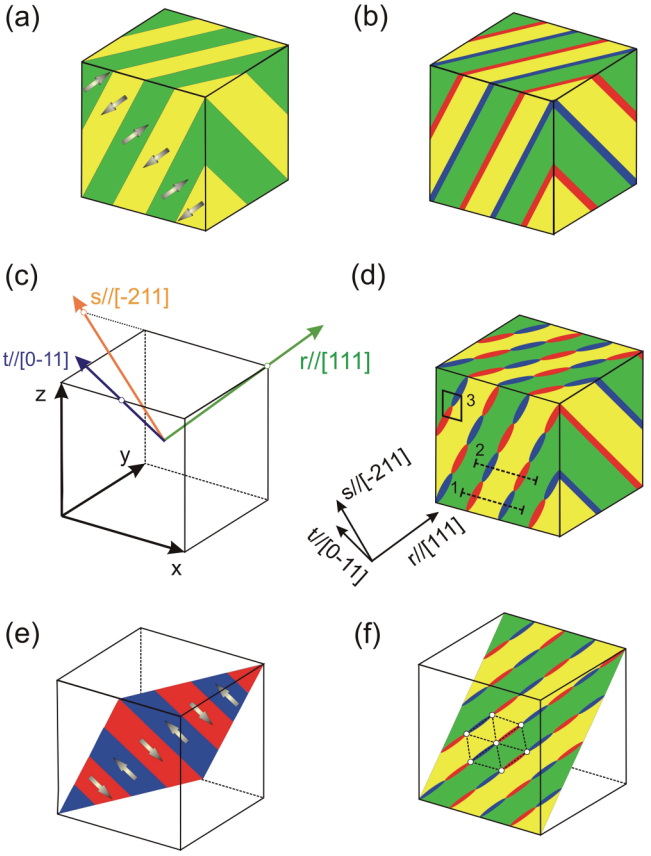

FIG. 2. (Color online) Plausible domain structures of rhombohedral $BaTiO_3$ with $[\bar{2}11]$-oriented 180° (a) Ising walls, (b) Bloch walls, and (d)–(f) Bloch walls containing Ising lines. (c) shows directions of the spontaneous polarization within ferroelectric domains (parallel or antiparallel to [111]), the internal polarization within the Bloch walls ($[01\bar{1}]$ or $[0\bar{1}1]$), and the domain-wall normal $\mathbf{s} \parallel [\bar{2}11]$. The distribution of the internal polarization within a selected Bloch wall is sketched in (e). Areas 1–3 marked in (d) relate to Figs. 3 and 4, and the hexagon shown in (f) emphasizes the Honeycomb lattice arrangement of Ising lines.

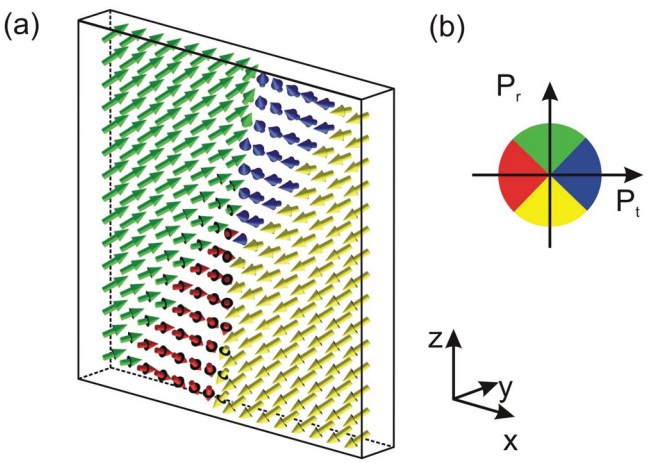

FIG. 3. (Color online) (a) Polarization around the Ising line in region 3 in Fig. 2(d), calculated at 0.5-nm mesh. (b) Domain-wall area, emphasized by the color code.

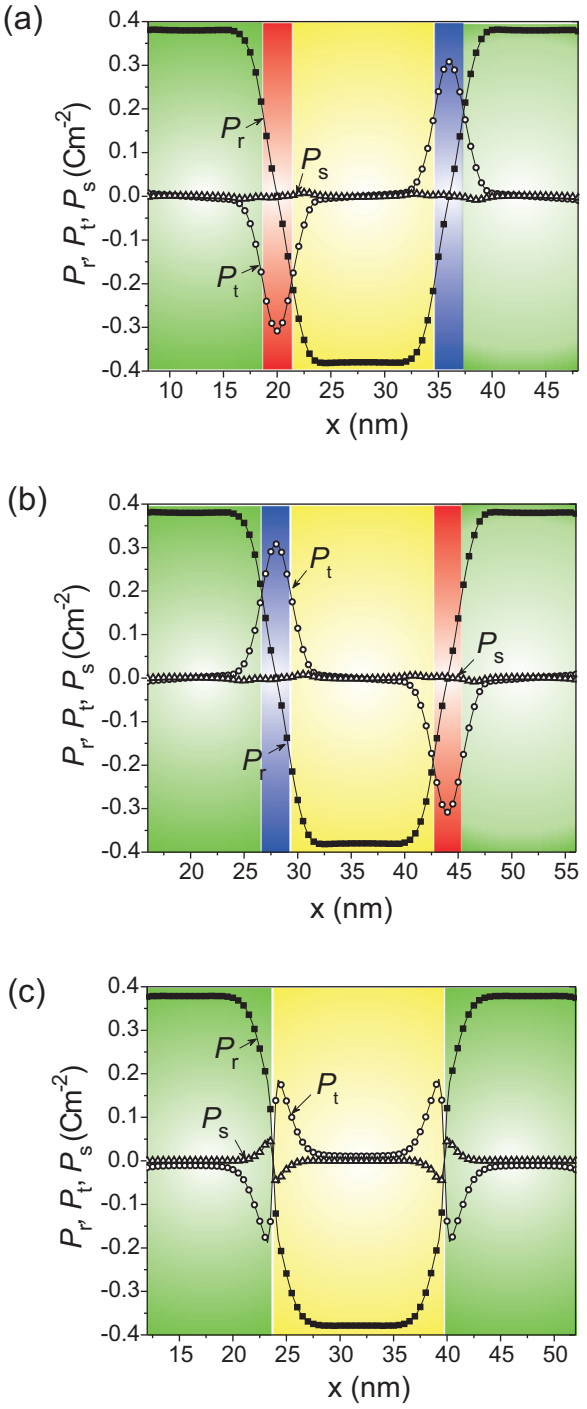

FIG. 4. (Color online) Profiles of P_r, P_t, and P_s polarization components along the [100] direction as obtained from phase-field simulations for rhombohedral $BaTiO_3$ at 118 K using the model described in the text. Data are taken from the front face of the simulation box (a) at the trajectory 1 and (b) at trajectory 2 shown in Fig. 2(d) and (c) at the intermediate trajectory passing through the Ising lines.

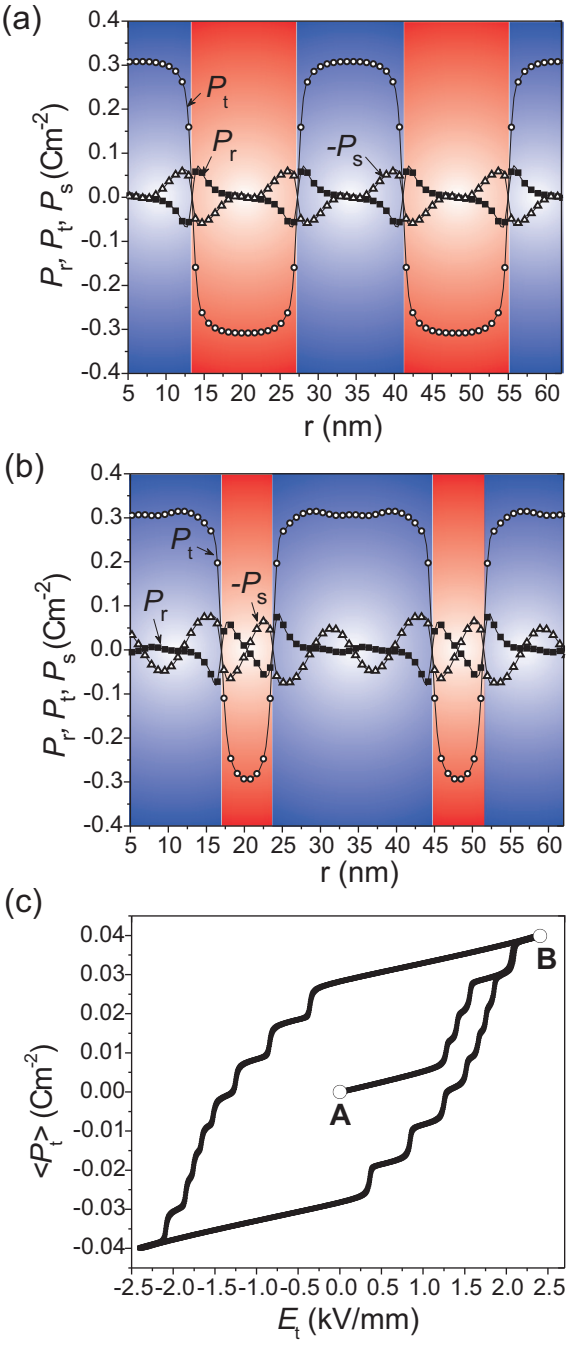

FIG. 5. (Color online) Profiles of the P_r, P_t, and P_s polarization components within a selected Bloch wall (along the $\mathbf{r} \parallel [111]$ direction) corresponding to (a) the virgin state and (b) the partially switched (b) state. These two states correspond to points A and B on (c) the quasistatic hysteresis loop, demonstrating switching of the domain-wall polarization $\mathbf{P}_{DW}$ by the electric field applied along the $\mathbf{t} \parallel [0\bar{1}1]$ direction. Results were obtained from phase-field simulations at 118 K using 128 × 128 × 128 simulation box with a spatial step of 0.5 nm.

$\mathbf{P}_{DW}$ really vanishes. This strongly contrasts with analogical line defects known from ferromagnetism. The reason for this difference is obviously the importance of the electrostatics; a ferroelectric Néel line would be strongly penalized by the associated local depolarization field [36]. However, this penalty is less prohibitive than that of the 2D Néel wall, and in principle, the ferroelectric Néel line may exist in some ferroelectric materials. It is likely that Ising-to-Néel or

Ising-to-Bloch crossover phenomena could occur in Ising lines curved or inclined out of their nominal orientation.

We have also explored the stability of the domain structure with respect to applied bias electric fields. The width of the Ising line is about 2 nm, and such a broad thickness ensures its high mobility within the domain wall. Concerted drift of Ising lines can be forced by a homogeneous bias field applied along the $\mathbf{t} \parallel [0\bar{1}1]$ direction. For example, in the simulations with a 0.5-nm step the coercive field sufficient to remove all the Ising lines at 118 K was only about 3 kV/mm.

A hysteresis loop showing variations of the P_t polarization component averaged over the whole supercell under a periodically oscillating electric field is shown in Fig. 5(c). This hysteresis is related to the growth of the area with a favorably oriented P_t component, mediated by the motion of the Ising lines. A comparison of the virgin and partially switched polarization profiles within the domain-wall plane is shown in Figs. 5(a) and 5(b). The profile of the P_t component clarifies that the Ising line can move as a soliton, without any essential change in its internal form.

Figure 5 also shows slight spatial oscillations of the profiles of P_s and P_r components. They are partially related to a slight bending of the domain-wall plane around the Ising line (the wall is not completely planar). On the other hand, the polarization profiles of the domain wall in the flat regions distant from the Ising line are very similar to the ideal polarization profiles obtained in Refs. [21,22]. In spite of a strong electrostatic interaction term in the model, domain-wall profiles in these flat regions [Figs. 4(a) and 4(b)] show a clear indication of the characteristic double kink in the normal (Néel) component of the polarization (P_s). It is worth noting that in some high-symmetry domain walls [37–39] such double kinks on P_s or P_t appear only after considering flexoelectric [40] coupling terms, while here, in the case of the $[\bar{2}11]$-oriented Bloch (bistable [41]) wall, the flexoelectric coupling has actually only a negligible influence on the domain-wall profile [21,22].

Since the polarization in our simulation happens to be strictly constant along the **t** direction, it is convenient to inspect the section of the simulated domain structure by a plane perpendicular to the $\mathbf{t} \parallel [0\bar{1}1]$ direction. The polarization distribution in this plane [highlighted in Fig. 2(f)] shows that here the Ising lines are actually forming a slightly distorted triangular lattice with mutual distances of about 14 nm. The macroscopic (average) symmetry of this relaxed domain structure is $2/m$, with the twofold axis along the **t** direction. However, the mirror symmetry plane here is actually a glide operation with a fractional translation along the **r** direction. Thus, it only transforms one Ising line to another one. This is compatible with the fact that the individual Ising line is a *chiral* object.

IV. DISCUSSION

In the continuum limit, the core of the Ising line is a line of zero polarization. In this sense, the Ising line cores are the lines of true singularities. The Jacobian matrix evaluated there has two complex-conjugate eigenvalues and one zero eigenvalue. Thus, the Ising line could be viewed as a line of focus-type singular points [42]. Moreover, it can be denoted as a vortex since it satisfies both the $Q > 0$ and $\lambda_2 < 0$ vortex identification criteria of Refs. [43,44], respectively [45,46]. Interestingly, Ising lines overall are slightly charged. The linear charge density of the perfectly $[0\bar{1}1]$-oriented Ising line studied here was less than about 10^{-10} C/m, but in principle, in a real material, it may play some role.

If we follow the polarization round an oriented circuit far from the core of a given Ising line (see Fig. 1), it is found that the polarization rotates once around the **s** direction [47]. Therefore, the Ising line can be considered an *edge* disclination of unit strength [13]. The nearest-neighbor Ising lines within the same domain wall have the opposite sense of the polarization rotation. In contrast, the flux closure vortices observed in ferroelectric thin films and ferroelectric nanodots are analogical to a *screw* disclination of unit strength because there the similar construction would result in rotation around the core of the vortex.

V. SUMMARY

In summary, we have explored properties of Ising lines – vortex line defects, expected to exist in ferroelectric Bloch walls as borderlines between areas of opposite helicity. We have proposed a simple ferroelectric domain structure with a triangular lattice of such Ising lines. This structure was shown to be stable within the established GLD model for rhombohedral phase of $BaTiO_3$.

In simple words, the Ising line studied here is an about 2-nm-thick, $[0\bar{1}1]$-oriented paraelectric nanorod of intrinsic nature, embedded within a $[\bar{2}11]$-oriented wall. This Ising line is mobile, and its motion mediates the switching of both the Bloch-wall helicity and Bloch-wall polarization. Therefore, the electric field parallel to the Ising line can be used to switch the domain-wall polarization without changing the bulk domain polarization. Obviously, it can be expected that when the electric field in such a direction is applied locally to an originally homogeneous Bloch wall, for example, using the tip of a conveniently designed atomic force microscope, then the Ising lines can also be created or destroyed in this way.

Finally, the structure of the Ising line itself was clarified. The polarization, followed along an oriented circuit drown around the axis of the Ising line (see Fig. 1), makes a full turn around the Bloch-wall normal **s**. Therefore, the structure of this vortex line differs from the more frequent case where the polarization rotates around the axis of the defect, for example, in two-dimensional skyrmions or the ferroelectric flux-closure vortices. The structure of the Ising line also differs from that of magnetic Bloch lines and Néel lines because the core of the Ising line is unpolarized. We believe that, in general, Ising lines with similar properties can be encountered in other kinds of ferroelectric Bloch walls.

ACKNOWLEDGMENT

This work is supported by the Czech Science Foundation (Project No. CSF 15-04121S).

[1] U. K. Rößler, A. N. Bogdanov, and C. Pfleiderer, Spontaneous skyrmion ground states in magnetic metals, Nature (London) **442**, 797 (2006).

[2] G. Catalan, J. Seidel, R. Ramesh, and J. F. Scott, Domain wall nanoelectronics, Rev. Mod. Phys. **84**, 119 (2012).

[3] A. N. Morozovska, E. A. Eliseev, and M. D. Glinchuk, Ferroelectricity enhancement in confined nanorods: Direct variational method, Phys. Rev. B **73**, 214106 (2006).

[4] S. Prosandeev and L. Bellaiche, Characteristics and signatures of dipole vortices in ferroelectric nanodots: First-principles-based simulations and analytical expressions, Phys. Rev. B **75**, 094102 (2007).

[5] I. Naumov and A. M. Bratkovsky, Unusual Polarization Patterns in Flat Epitaxial Ferroelectric Nanoparticles, Phys. Rev. Lett. **101**, 107601 (2008).

[6] J. Slutsker, A. Artemev, and A. Roytburd, Phase-Field Modeling of Domain Structure of Confined Nanoferroelectrics, Phys. Rev. Lett. **100**, 087602 (2008).

[7] A. Gruverman, D. Wu, H.-J. Fan, I. Vrejoiu, M. Alexe, R. J. Harrison, and J. F. Scott, Vortex ferroelectric domains, J. Phys. Condens. Matter **20**, 342201 (2008).

[8] N. Balke, S. Choudhury, S. Jesse, M. Huijben, Y. H. Chu, A. P. Baddorf, L. Q. Chen, R. Ramesh, and S. V. Kalinin, Deterministic control of ferroelastic switching in multiferroic materials, Nat. Nanotechnol. **4**, 868 (2009).

[9] M. G. Stachiotti and M. Sepliarsky, Toroidal Ferroelectricity in $PbTiO_3$ Nanoparticles, Phys. Rev. Lett. **106**, 137601 (2011).

[10] L. Baudry, A. Sené, I. A. Luk'yanchuk, and L. Lahoche, Vortex state in thin films of multicomponent ferroelectrics, Thin Solid Films **519**, 5808 (2011).

[11] L. Louis, I. Kornev, G. Geneste, B. Dkhil, and L. Bellaiche, Novel complex phenomena in ferroelectric nanocomposites, J. Phys. Condens. Matter **24**, 402201 (2012).

[12] S.-Z. Lin, X. Wang, Y. Kamiya, G.-W. Chern, F. Fan, D. Fan, B. Casas, Y. Liu, V. Kiryukhin, W. H. Zurek, C. D. Batista, and S.-W. Cheong, Topological defects as relics of emergent continuous symmetry and Higgs condensation of disorder in ferroelectrics, Nat. Phys. **10**, 970 (2014).

[13] F. R. N. Nabarro, Singular lines and singular points of ferromagnetic spin systems and of nematic liquid crystals, J. Phys. (Paris) **33**, 1089 (1972).

[14] L. Lejček, M. Glogarová, and J. Pavel, Twist disclinations in thin SmC^* liquid crystal, Phys. Status Solidi A **82**, 47 (1984).

[15] A. P. Malozemoff and J. C. Slonczewski, *Magnetic Domain Walls in Bubble Materials* (Academic, New York, 1979).

[16] S. Middelhoek, Domain walls in thin Ni–Fe films, J. Appl. Phys. **34**, 1054 (1963).

[17] L. Néel, Energie des parois de Bloch dans les couches minces, C. R. Acad. Sci. (Paris) **241**, 533 (1955).

[18] A. Hubert and R. Schäfer, *Magnetic Domains: The Analysis of a Magnetic Microstructures* (Springer, Berlin, 1998).

[19] P. Marton, I. Rychetsky, and J. Hlinka, Domain walls of ferroelectric $BaTiO_3$ within the Ginzburg-Landau-Devonshire phenomenological model, Phys. Rev. B **81**, 144125 (2010).

[20] J. Hlinka, V. Stepkova, P. Marton, I. Rychetsky, V. Janovec, and P. Ondrejkovic, Phase-field modelling of 180° "Bloch walls" in rhombohedral $BaTiO_3$, Phase Transitions **84**, 738 (2011).

[21] V. Stepkova, P. Marton, and J. Hlinka, Stress-induced phase transition in ferroelectric domain walls of $BaTiO_3$, J. Phys. Condens. Matter **24**, 212201 (2012).

[22] E. A. Eliseev, P. V. Yudin, S. V. Kalinin, N. Setter, A. K. Tagantsev, and A. N. Morozovska, Structural phase transitions and electronic phenomena at 180-degree domain walls in rhombohedral $BaTiO_3$, Phys. Rev. B **87**, 054111 (2013).

[23] M. Taherinejad, D. Vanderbilt, P. Marton, V. Stepkova, and J. Hlinka, Bloch-type domain walls in rhombohedral $BaTiO_3$, Phys. Rev. B **86**, 155138 (2012).

[24] J. C. Wojdeł and J. Íñiguez, Ferroelectric Transitions at Ferroelectric Domain Walls Found from First Principles, Phys. Rev. Lett. **112**, 247603 (2014).

[25] J. Hlinka and P. Marton, Phenomenological model of a 90° domain wall in $BaTiO_3$-type ferroelectrics, Phys. Rev. B **74**, 104104 (2006).

[26] J. Hlinka, P. Ondrejkovic, and P. Marton, The piezoelectric response of nanotwinned $BaTiO_3$, Nanotechnology **20**, 105709 (2009).

[27] P. Marton, V. Stepkova, and J. Hlinka, Divergence of dielectric permittivity near phase transition within ferroelectric domain boundaries, Phase Transitions **86**, 103 (2013).

[28] J. Lajzerowicz and J. J. Niez, Phase transition in a domain wall, J. Phys. (Paris) Lett. **40**, L165 (1979).

[29] E. K. H. Salje and J. F. Scott, Ferroelectric Bloch-line switching: A paradigm for memory devices? Appl. Phys. Lett. **105**, 252904 (2014).

[30] É. B. Sonin and A. K. Tagantsev, Circulation lines and motion of antiphase boundaries in an improper ferroelectric, Zh. Eksp. Teor. Fiz. **94**, 315 (1988) [Sov. Phys. JETP **67**, 396 (1988)], http://www.jetp.ac.ru/cgi-bin/e/index/e/67/2/p396?a=list.

[31] P. Marton and J. Hlinka, Simulation of domain patterns in $BaTiO_3$, Phase Transitions **79**, 467 (2006).

[32] H.-L. Hu and L.-Q. Chen, Three-dimensional computer simulation of ferroelectric domain formation, J. Am. Ceram. Soc. **81**, 492 (1998).

[33] S. Semenovskaya and A. G. Khachaturyan, Development of ferroelectric mixed states in a random field of static defects, J. Appl. Phys. **83**, 5125 (1998).

[34] S. Nambu and D. A. Sagala, Domain formation and elastic long-range interaction in ferroelectric perovskites, Phys. Rev. B **50**, 5838 (1994).

[35] C. Kittel, Physical theory of ferromagnetic domains, Rev. Mod. Phys. **21**, 541 (1949).

[36] A. P. Levanyuk and R. Blinc, Ferroelectric Phase Transitions in Small Particles and Local Regions, Phys. Rev. Lett. **111**, 097601 (2013).

[37] P. V. Yudin, A. K. Tagantsev, E. A. Eliseev, A. N. Morozovska, and N. Setter, Bichiral structure of ferroelectric domain walls driven by flexoelectricity, Phys. Rev. B **86**, 134102 (2012).

[38] M. Li, Y. Gu, Y. Wang, L.-Q. Chen, and W. Duan, First-principles study of 180° domain walls in $BaTiO_3$: Mixed Bloch-Néel-Ising character, Phys. Rev. B **90**, 054106 (2014).

[39] Y. Gu, M. Li, A. N. Morozovska, Y. Wang, E. A. Eliseev, V. Gopalan, and L.-Q. Chen, Flexoelectricity and ferroelectric domain wall structures: Phase-field modeling and DFT calculations, Phys. Rev. B **89**, 174111 (2014).

[40] P. V. Yudin and A. K. Tagantsev, Fundamentals of flexoelectricity in solids, Nanotechnology **24**, 432001 (2013).

[41] P. V. Yudin, A. K. Tagantsev, and N. Setter, Bistability of ferroelectric domain walls: Morphotropic boundary and strain effects, Phys. Rev. B **88**, 024102 (2013).

[42] H. Poincaré, Sur les courbes définies par les équations différentielles (IV), J. Math. Pures Appl. **2**, 151 (1886).

[43] J. C. R. Hunt, A. A. Wray, and P. Moin, Eddies, stream, and convergence zones in turbulent flows, Center for Turbulence Research Report No. CTR-S88 (1988), pp. 193–208.

[44] J. Jeong and F. Hussain, On the identification of a vortex, J. Fluid Mech. **285**, 69 (1995).

[45] V. Kolář, J. Šístek, F. Cirak, and P. Moses, Average corotation of line segments near a point and vortex identification, AIAA J. **51**, 2678 (2013).

[46] F. H. Post, B. Vrolijk, H. Hauser, R. S. Laramee, and H. Doleisch, The state of the art in flow visualisation: Feature extraction and tracking, Comput. Graphics Forum **22**, 775 (2003).

[47] N. D. Mermin, The topological theory of defects in ordered media, Rev. Mod. Phys. **51**, 591 (1979).